THE JOURNAL OF PHYSICAL CHEMISTRY C

Article

pubs.acs.org/JPCC

Floating Patches of HCN at the Surface of Their Aqueous Solutions – Can They Make "HCN World" Plausible?

Balázs Fábián,[†,‡] Milán Szőri,*[,§] and Pál Jedlovszky*[,†,∥,⊥]

[†]Laboratory of Interfaces and Nanosize Systems, Institute of Chemistry, Eötvös Loránd University, Pázmány P. Stny 1/A, H-1117 Budapest, Hungary

[‡]Department of Inorganic and Analytical Chemistry, Budapest University of Technology and Economics, Szt. Gellért tér 4, H-1111 Budapest, Hungary

[§]Department of Chemical Informatics, Faculty of Education, University of Szeged, Boldogasszony sgt. 6, H-6725 Szeged, Hungary

[∥]MTA-BME Research Group of Technical Analytical Chemistry, Szt. Gellért tér 4, H-1111 Budapest, Hungary

[⊥]EKF Department of Chemistry, Leányka utca 6, H-3300 Eger, Hungary

Supporting Information

ABSTRACT: The liquid/vapor interface of the aqueous solutions of HCN of different concentrations has been investigated using molecular dynamics simulation and intrinsic surface analysis. Although HCN is fully miscible with water, strong interfacial adsorption of HCN is observed at the surface of its aqueous solutions, and, at the liquid surface, the HCN molecules tend to be located even at the outer edge of the surface layer. It turns out that in dilute systems the HCN concentration can be about an order of magnitude larger in the surface layer than in the bulk liquid phase. Furthermore, HCN molecules show a strong lateral self-association behavior at the liquid surface, forming thus floating HCN patches at the surface of their aqueous solutions. Moreover, HCN molecules are staying, on average, an order of magnitude longer at the liquid surface than water molecules, and this behavior is more pronounced at smaller HCN concentrations. Because of this enhanced dynamical stability, the floating HCN patches can provide excellent spots for polymerization of HCN, which can be the key step in the prebiotic synthesis of partially water-soluble adenine. All of these findings make the hypothesis of "HCN world" more plausible.

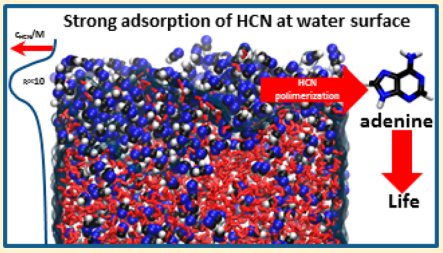

1. INTRODUCTION

Atmospheric hydrogen cyanide (HCN), a simple endothermic species, is produced primarily in biomass burning as a result of pyrolysis of N-containing compounds. Although it has a high natural variability in HCN emissions even within a single or similar fire types, it is often used as a tracer of pollution originating from wildfires[1−3] to deconvolute mixtures of urban and biomass burning emissions.[4] Besides biomass burning, atmospheric HCN has also been formed in lightning perturbed air in the troposphere of the modern Earth,[5,6] making lightning an additional source of HCN.[7] Considering the budget of atmospheric HCN, its direct photolysis is apparently negligible; the estimated photochemical lifetime of HCN is around 10 years or even more in the stratosphere below 30 km, and around 5 years in the upper troposphere.[8] However, global satellite observations of HCN in the upper troposphere[9] reveal the clear signature of air depleted in HCN over the tropical oceans.[10] Therefore, the uptake into the ocean via wet deposition is currently known to be the dominant sink with an inferred global HCN biomass burning source of 1.4−2.9 Tg(N)/year and an oceanic saturation ratio of 0.83.[11] Because of this oceanic loss, the lifetime of HCN reduces to 2−5 months,[2,3,11] and it is thought to be an important source of nitrogen in remote oceanic environments.[11] Alternative stratospheric loss of HCN, in which reactions with OH and $O(^1D)$ are dominated, can be assumed to be less pronounced.[8,12]

The aforementioned formation of HCN by lightning does not only occur in the modern atmosphere, but happened also in the atmosphere of prebiotic Earth. The pioneering experiment by Miller and Urey,[13] in which amino acids are readily formed from methane, ammonia, and water subjected to electric discharges, has naturally strengthened the widespread assumption that the original formation of primitive proteins occurred through the polycondensation of these monomers, although the amino acids are actually secondary products arising from polypeptides formed by way of polymerization of HCN.[14,15] Such formation of HCN is not a unique feature of the Miller−Urey setup; it can occur by electric discharges from many diverse mixtures of gases, including $CO-N_2-H_2$ and $CO_2-N_2-H_2O$.[16,17] Therefore, HCN is considered to have been an important source of biological molecules on the primitive Earth.[18−22] After the uptake of HCN in water, two chemical processes are assumed to occur: the polymerization (probably to biomolecules) and the hydrolysis of HCN to NH_2CHO.

Received: June 16, 2014
Revised: August 11, 2014
Published: August 14, 2014

   dx.doi.org/10.1021/jp505978p | J. Phys. Chem. C 2014, 118, 21469−21482

Generally speaking, the hydrolysis predominates in dilute solutions, while polymerization takes over at higher concentrations.[23] Oligomerization of HCN is of particular interest because adenine is an essential nucleobase, and formally it is the pentamer of HCN.[16,24,25] Several amino acids and peptides can also be synthesized through the oligomerization of HCN followed by hydrolysis, which supports the hypothesis of the so-called "HCN world".[15,26] Nevertheless, adenine can be detected only in concentrated (1−11 M) aqueous solutions of HCN.[27,28] Thus, the main criticism concerning the "HCN world" hypothesis is that the bulk concentration of HCN in the primitive ocean was estimated to be far too low for polymerization, and hence hydrolysis to NH_2CHO could have been favored instead.[29,30] Solely on the basis of this evidence, it is less plausible that prebiotic formation of the biomolecular building blocks via the oligomerization could happen in the bulk phase due to the issue with HCN concentration. Air/ice[31] and air/water interfaces can, however, be alternative locations for possible enrichment of HCN where oligomerization could have taken place. Because of the fact that HCN is a highly water-soluble weak acid, only its bulk phase properties are usually considered. It was shown recently that molecular HCl, which possesses strong acidity, has a very strong propensity for the air−water interface.[32] The question can thus arise that HCN also has significant enrichment at the surface of its aqueous solution regardless of its weaker acidic character.

Computer simulation methods seem to be particularly suitable to address this question, because in a computer simulation a full, atomistic level insight is gained to the structure of the appropriately chosen model of the system of interest. However, when the surface of a liquid phase is seen at atomistic resolution, as is in computer simulations, the detection of the exact location of the liquid surface (or, equivalently, the distinction between interfacial and non-interfacial molecules) is far from being a trivial task. The problem originates from the fact that the liquid surface is corrugated by capillary waves at the atomistic length scale. Defining the interface simply as a slab parallel with its macroscopic plane, as done in many of the early simulations, is repeatedly shown to lead to systematic error of unknown magnitude not only in the structural properties of the interface,[33,34] but also in its composition (i.e., extent of adsorption of certain components)[35−37] and even in some of the thermodynamic properties of the system.[38] To overcome this problem, several methods have been proposed in the past decade,[33,39−43] among which the method called Identification of the Truly Interfacial Molecules (ITIM)[33] turned out to be an excellent compromise between computing time and accuracy.[44] The ITIM method has successfully been applied to describe the liquid−vapor interface of various aqueous mixtures[35−37,45] as well as that of other systems[33,46−50] and various water−organic liquid−liquid interfaces.[34,38,51,52] It has also been used to calculate the intrinsic solvation free energy profile (i.e., that relative to the real, capillary wave corrugated liquid surface) of various penetrants across liquid−liquid interfaces,[53,54] and proved to be essential in explaining the surface tension anomaly of neat water.[55]

In this Article, we present computer simulation results of the liquid−vapor interface of water−HCN mixtures of six different compositions, covering the HCN mole percentage range from 3% to 30%. As it turns out, due to the strong adsorption of HCN at the liquid surface, these systems practically cover the entire composition range for the surface layer. For reference, simulations of the two neat systems are also reported here. The surface layer of the liquid phase is identified in the simulations by means of the ITIM method, and its properties (i.e., width, roughness, orientation of the surface molecules, adsorption and lateral self-association of HCN in the surface layer, dynamics of exchange of the molecules between the surface layer and the bulk liquid phase) are analyzed in detail. Particular emphasis is given to properties that can be relevant with respect to a possible HCN oligomerization at the surface of its dilute aqueous solution. The results obtained for the first molecular layer beneath the liquid surface are also compared to those obtained for the subsequent subsurface molecular layers.

This Article is organized as follows. In section 2, details of the computer simulations and ITIM analyses performed are given. The obtained results, concerning both the properties of the entire surface layer and also those of the molecules belonging to it, are presented and detailed in section 3. Finally, in section 4 the main conclusions of this study are summarized, and the relevance of the present results with respect to the possible polymerization of HCN under prebiotic conditions is addressed.

2. COMPUTATIONAL DETAILS

Molecular dynamics simulations of the liquid−vapor interface of water−HCN mixtures of different compositions have been performed on the canonical (N,V,T) ensemble at the temperature of 273 K. The X, Y, and Z edges of the rectangular basic simulation box have been 300, 50, and 50 Å, respectively; edge X has been perpendicular to the macroscopic plane of the interface. Standard periodic boundary conditions have been applied. The basic box consisted of 4000 molecules, among which 0, 120, 200, 400, 600, 800, 1200, and 4000 have been HCN in the different simulations. These systems are referred to here as the 0% HCN, 3% HCN, 5% HCN, 10% HCN, 15% HCN, 20% HCN, 30% HCN, and 100% HCN system, respectively.

HCN molecules have been described by the potential model of Kotdawala et al.,[56] based on the OPLS force field,[57,58] in which the C−H and C≡N bonds are 1.068 and 1.157 Å long, respectively, and the three atomic sites are arranged linearly. Excepting the small deviations from linearity of the HCN monomers predicted by Born−Oppenheimer molecular dynamics, both the first-principles and the classical molecular dynamics (where a rigid and nonpolarizable model was adopted) predict similar structures for liquid HCN.[59] Because HCN is a weak acid, that is, its pK_a value is 9.2, less than 1% of the HCN molecules is ionized in the acidic pH range; therefore, the presence of one single CN^- ion would already be an overrepresentation even for the most concentrated HCN solution considered here (corresponding to the HCN mole percentage of 30%). Water molecules have been modeled by the TIP4P potential.[60]

The total potential energy of the system has been calculated as the sum of the interaction energies of all molecule pairs; and the interaction energy of molecule i and j, u_{ij}, has been calculated as

$$u_{ij} = \sum_{\alpha}^{n_i} \sum_{\beta}^{n_j} \frac{1}{4\pi\varepsilon_0} \frac{q_\alpha q_\beta}{r_{i\alpha,j\beta}} + 4\varepsilon_{\alpha\beta}\left[\left(\frac{\sigma_{\alpha\beta}}{r_{i\alpha,j\beta}}\right)^{12} - \left(\frac{\sigma_{\alpha\beta}}{r_{i\alpha,j\beta}}\right)^{6}\right] \quad (1)$$

dx.doi.org/10.1021/jp505978p | J. Phys. Chem. C 2014, 118, 21469−21482

In this equation, indices α and β run over the n_i and n_j interaction sites of molecules i and j, respectively, q_α and q_β are the fractional charges carried by the respective interaction sites, ε_0 is the vacuum permittivity, $r_{i\alpha,j\beta}$ is the distance of site α of molecule i from site β of molecule j, and $\varepsilon_{\alpha\beta}$ and $\sigma_{\alpha\beta}$ are the energy and distance parameters, respectively, of the Lennard-Jones interaction between sites α and β, related to the parameters corresponding to the individual sites through the Lorentz–Berthelot rule,[61] i.e.,:

$$\varepsilon_{\alpha\beta} = \sqrt{\varepsilon_\alpha \varepsilon_\beta} \tag{2}$$

and

$$\sigma_{\alpha\beta} = \frac{\sigma_\alpha + \sigma_\beta}{2} \tag{3}$$

The interaction parameters q, σ, and ε corresponding to the different sites of the HCN and water models used are collected in Table 1. All interactions have been truncated to zero beyond the center–center cutoff distance of 15 Å; the long-range part of the Coulombic interaction of the fractional charges has been taken into account by the Particle Mesh Ewald (PME) method.[62]

Table 1. Interaction Parameters of the Potential Models Used

molecule	site	q/e	σ/Å	(ε/k_B)/K
HCN[a]	H	0.15	0.0	0.0
	C	0.28	3.63	77.0
	N	−0.43	3.20	88.0
water[b]	O	0.0	3.154	78.06
	H	0.52	0.0	0.0
	M[c]	−1.04	0.0	0.0

[a]Reference 56. [b]TIP4P model, ref 60. [c]Nonatomic interaction site, placed along the H–O–H bisector 0.15 Å away from the O atom.

The simulations have been performed by the GROMACS 4.5.5 program package.[63] The temperature of the system has been controlled using the Nosé–Hoover thermostat.[64,65] According to the potential models used, both the HCN and the water molecules have been treated as rigid bodies in the simulations; their geometries have been kept unchanged by means of the LINCS[66] and SETTLE[67] algorithms, respectively. The equations of motion have been integrated in time steps of 1 fs. Initial configurations have been created in the following way. First, the required number of molecules have been placed in a basic box, the Y and Z edges of which have already been 50 Å, while the length of the X edge has roughly corresponded to the density of the liquid phase. After proper energy minimization, the systems have been equilibrated for 2 ns on the isothermal–isobaric (N,p,T) ensemble at 1 bar. The liquid–vapor interface has then been created by increasing the length of the X edge to 300 Å. The interfacial system has been further equilibrated, already on the (N,V,T) ensemble, for another 2 ns. Finally, 2000 sample configurations, separated by 1 ps long trajectories each, have been dumped for further analyses during the 2 ns long production stage of the simulations. The surface tensions of the systems studied are collected in Table 2, as obtained from the simulations.

The molecules constituting the first layer of the liquid phase have been identified by means of the ITIM method,[33] i.e., by moving a probe sphere along test lines perpendicular to the macroscopic plane of the interface, YZ, from the bulk vapor phase toward the interface. The molecules that are first hit by the probe sphere along any of the test lines (i.e., the ones "seen" by the probe from the vapor phase) are considered as being at the interface. Test lines, being parallel with edge X of the basic box, have been arranged in a 100 × 100 grid along the YZ plane; thus, two neighboring test lines have been separated by 0.5 Å. According to the suggestion of Jorge et al.,[44] the radius of the probe sphere has been set to 1.25 Å. To determine when a molecule is touched by the probe, the atoms have been approximated by spheres, the diameters of which have been equal to the corresponding Lennard-Jones distance parameter, σ. This way, H atoms have been omitted from the ITIM analysis (see Table 1). Finally, by disregarding the molecules identified as forming the surface layer and repeating the entire procedure twice more, the molecules forming the second and the third layer beneath the liquid surface have also been identified. An equilibrium snapshot of the 20% HCN system, indicating also the molecules forming the first three subsurface molecular layers as identified by ITIM, is shown in Figure 1.

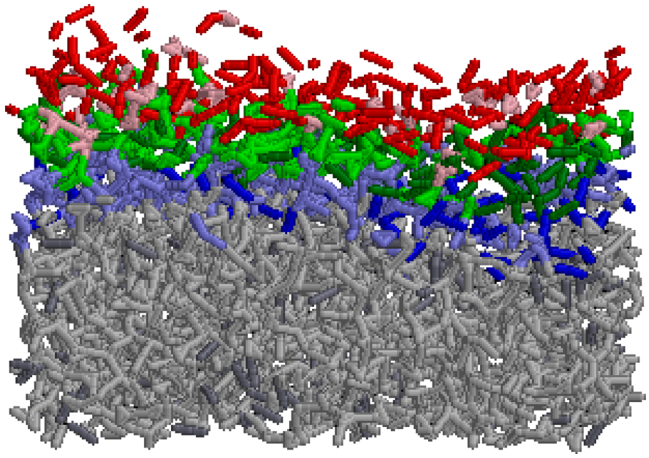

Figure 1. Equilibrium snapshot of the 20% HCN system, as taken out from the simulation. Molecules belonging to the first, second, and third subsurface molecular layers as well as to the bulk liquid phase are marked by red, green, blue, and gray colors, respectively. Darker and lighter shades of the colors correspond to the HCN and water molecules, respectively. The snapshot only shows the $X > 0$ Å half of the basic box.

3. RESULTS AND DISCUSSION

3.1. Properties of the Surface Layer. The number density profiles of the water and HCN molecules along the macroscopic surface normal axis, X, in selected systems

Table 2. Surface Tension of the Systems Simulated

system	0% HCN	3% HCN	5% HCN	10% HCN	15% HCN	20% HCN	30% HCN	100% HCN
γ/mN m^{-1}	57.8[a]	52.8	51.3	44.2	41.8	37.9	35.9	31.0[b]

[a]Experimental value is 72.3 mN/m at 296 K, ref 68. [b]Experimental value is 19.7 mN/m at 293 K, ref 69.

dx.doi.org/10.1021/jp505978p | J. Phys. Chem. C 2014, 118, 21469–21482

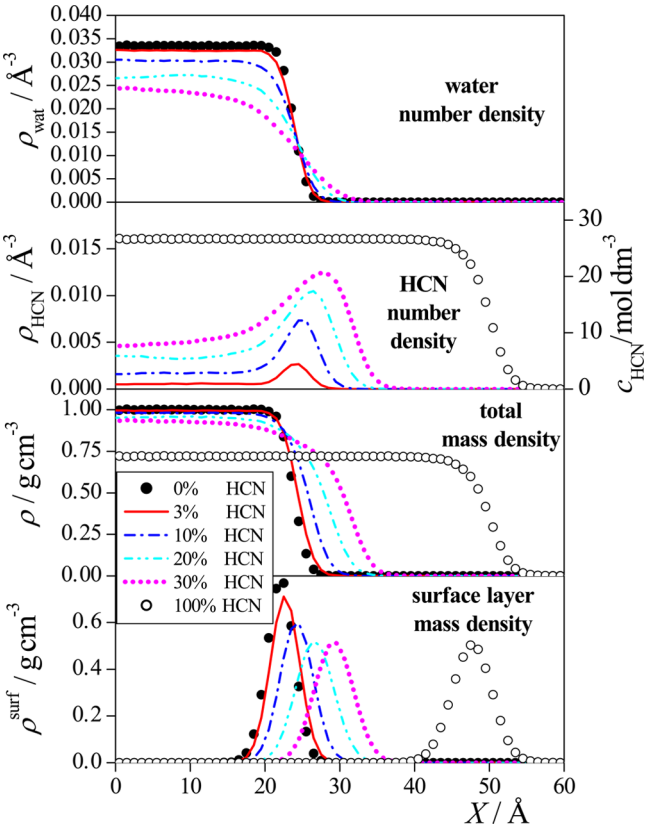

Figure 2. Number density profile of the water (top panel) and HCN (second panel) molecules as well as mass density of the entire system (third panel) and its surface layer (bottom panel) along the macroscopic surface normal axis X in the systems containing 0% HCN (●), 3% HCN (red solid lines), 10% HCN (dark blue dash–dotted lines), 20% HCN (light blue dash–dot–dotted lines), 30% HCN (magenta dotted lines), and 100% HCN (○). All profiles shown are symmetrized over the two liquid–vapor interfaces present in the basic simulation box. The scale on the right of the second panel refers to the concentration (molarity) of HCN.

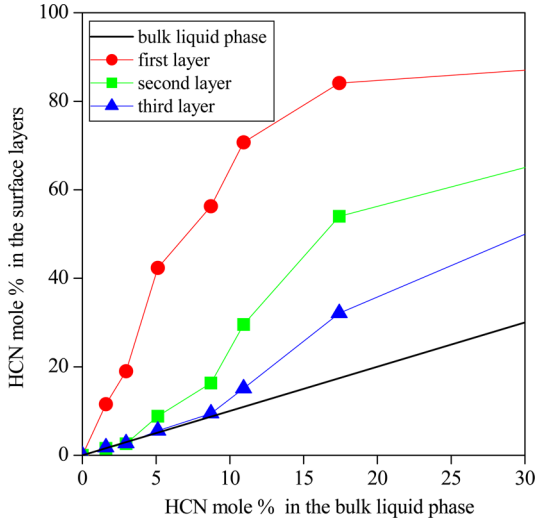

Figure 3. Composition (in terms of HCN mole percentage) of the first (red ●), second (green ■), and third (blue ▲) subsurface molecular layers as well as of the bulk liquid phase (black solid line) as a function of the composition of the bulk liquid phase in the systems simulated.

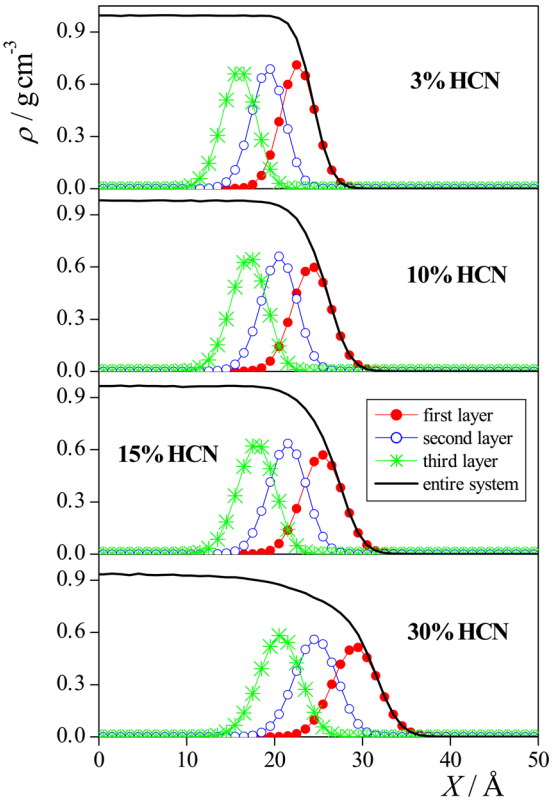

Figure 4. Mass density profile of the entire system (black solid lines) as well as its first (red ●), second (blue ○), and third (green asterisks) subsurface molecular layers along the macroscopic surface normal axis X in the systems containing 3% HCN (top panel), 10% HCN (second panel), 15% HCN (third panel), and 30% HCN (bottom panel). All profiles shown are symmetrized over the two liquid–vapor interfaces present in the basic simulation box.

simulated are shown in Figure 2, along with the mass density profiles of the entire systems and of their surface layers. As is seen, while the water density drops monotonically from the bulk liquid phase value to practically zero, the HCN profiles go through a clear maximum around the location of the first molecular layer. In other words, HCN molecules are strongly adsorbed at the surface of the liquid phase. To quantify the extent of this adsorption, we have plotted the HCN mole percentage in the first three molecular layers against the HCN mole percentage in the bulk liquid phase in Figure 3. It should be noted that the HCN mole percentage in the bulk phase is not equal to the overall HCN mole percentage in the system; it has simply been determined from the ratio of the constant, bulk liquid phase values of the HCN, and water number density profiles.

As is clearly seen from Figure 3, the adsorption of HCN is rather strong; in dilute systems the HCN concentration can be about an order of magnitude larger in the surface layer than in the bulk liquid phase. Further, in the 30% HCN system, in which the bulk phase HCN mole percentage is about 17%, more than 80% of the surface molecules are HCN. It is also seen that our systems simulated cover rather uniformly the entire composition range of the surface layer. Another important finding is that as the bulk phase HCN concentration increases, the adsorption gradually involves more subsurface layers. Thus, above the bulk percentages of 5% and 10% (corresponding to the 10% HCN and 20% HCN systems), even the second and third molecular layers beneath the surface,

dx.doi.org/10.1021/jp505978p | J. Phys. Chem. C 2014, 118, 21469–21482

Table 3. Calculated Properties of the First Three Subsurface Molecular Layers of the Systems Simulated

						τ/ps	
subsurface layer	system	δ/Å	X_c/Å	ξ	a/Å	water	HCN
first layer	0% HCN	3.66	22.08	1.09	2.12	29.4	
	3% HCN	3.91	22.66	1.22	2.31	26.20	200.1
	5% HCN	4.03	23.11	1.27	2.36	21.24	167.2
	10% HCN	4.41	24.23	1.35	2.55	13.86	77.67
	15% HCN	4.65	25.41	1.34	2.72	10.88	55.80
	20% HCN	5.09	26.64	1.35	2.82	9.23	39.26
	30% HCN	5.16	29.20	1.41	2.96	8.78	28.81
	100% HCN	5.33	47.69	1.34	3.03		22.55
second layer	0% HCN	3.65	18.71	1.00	2.08	2.21	
	3% HCN	3.80	19.24	1.03	2.16	2.10	7.86
	5% HCN	3.86	19.63	1.05	2.20	2.00	6.88
	10% HCN	4.09	20.50	1.10	2.33	2.16	4.33
	15% HCN	4.29	21.47	1.11	2.48	2.62	3.52
	20% HCN	4.69	22.42	1.15	2.61	3.45	4.14
	30% HCN	4.86	24.67	1.23	2.74	3.26	3.86
	100% HCN	5.23	42.78	1.21	2.90		1.86
third layer	0% HCN	3.73	15.46	1.04	2.10	2.28	
	3% HCN	3.85	15.94	1.04	2.17	2.28	10.51
	5% HCN	3.90	16.29	1.05	2.21	2.22	8.21
	10% HCN	4.09	17.05	1.07	2.32	2.15	5.76
	15% HCN	4.26	17.90	1.06	2.45	2.12	3.56
	20% HCN	4.59	18.68	1.07	2.59	2.24	3.74
	30% HCN	4.73	20.58	1.14	2.71	2.78	3.48
	100% HCN	5.21	37.97	1.16	2.94		1.82

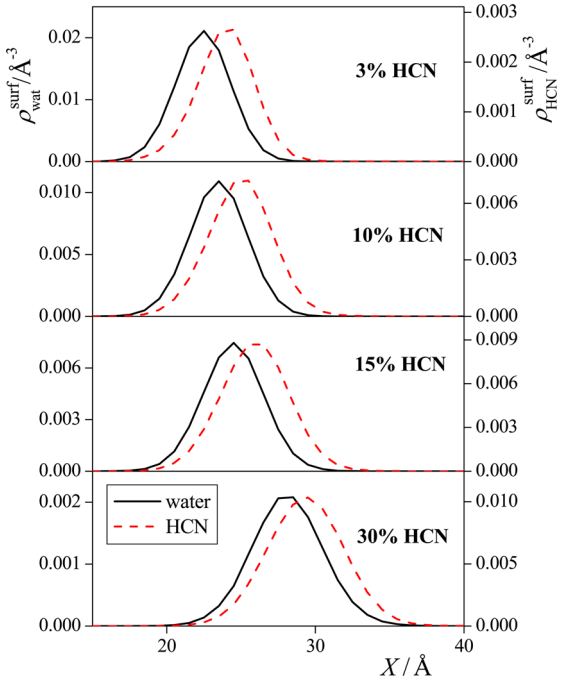

Figure 5. Number density profile of the water (black solid lines) and HCN (red dashed lines) molecules of the first subsurface molecular layer along the macroscopic surface normal axis X in the systems containing 3% HCN (top panel), 10% HCN (second panel), 15% HCN (third panel), and 30% HCN (bottom panel). The scales on the left and right of the panels refer to the water and HCN densities, respectively. All profiles shown are symmetrized over the two liquid–vapor interfaces present in the basic simulation box.

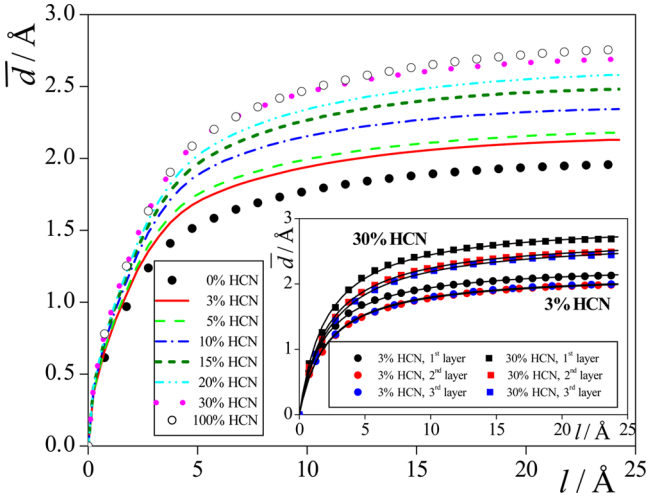

Figure 6. Average normal distance of two surface points as a function of their lateral distance, as obtained in the systems containing 0% HCN (●), 3% HCN (red solid lines), 5% HCN (light green dashed lines), 10% HCN (dark blue dash–dotted lines), 15% HCN (dark green short dashed lines), 20% HCN (light blue dash–dot–dotted lines), 30% HCN (magenta dotted lines), and 100% HCN (○). The inset shows the average normal distance versus lateral distance data in the first (black symbols), second (red symbols), and third (blue symbols) subsurface molecular layers of the systems containing 3% HCN (circles) and 30% HCN (squares). The curves fitted to the data according to eq 4 are shown by solid lines.

respectively, are noticeably richer in HCN than the bulk liquid phase. This behavior is in a clear contrast with that of methanol and dimethyl sulfoxide, the adsorption of which was shown to be extended solely to the first molecular layer in their aqueous solutions.[35,37] On the other hand, similar multilayer adsorption was observed previously for acetonitrile,[36] a molecule homologous with HCN. The multilayer adsorption of

dx.doi.org/10.1021/jp505978p | J. Phys. Chem. C 2014, 118, 21469–21482

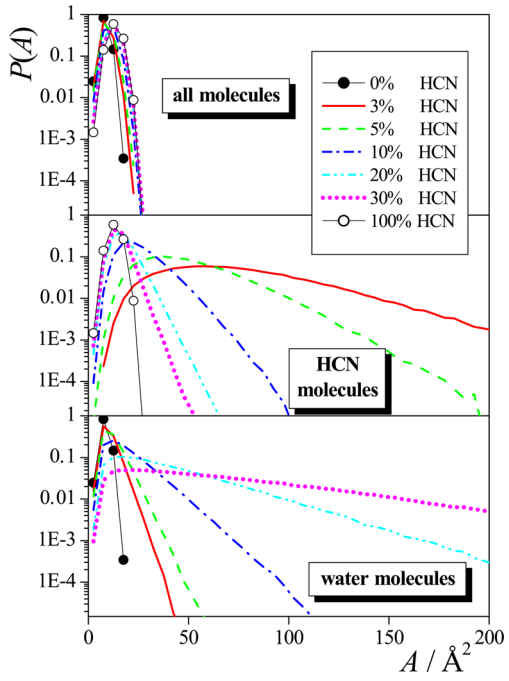

Figure 7. Distribution of the Voronoi polygon area of the molecules in the surface layer, as calculated regarding all surface molecules (top panel), only the HCN molecules of the surface layer (middle panel), and only the water molecules of the surface layer (bottom panel) in the systems containing 0% HCN (●), 3% HCN (red solid lines), 5% HCN (green dashed lines), 10% HCN (dark blue dash−dotted lines), 20% HCN (light blue dash−dot−dotted lines), 30% HCN (magenta dotted lines), and 100% HCN (○). In the calculation, the molecules have been represented by their centers projected to the macroscopic plane of the surface (see the text). To emphasize the exponential decay of the curves, the data are shown on a logarithmic scale.

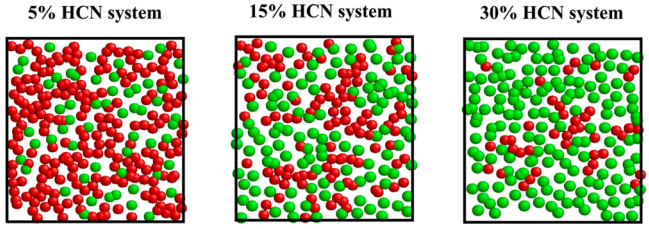

Figure 8. Instantaneous snapshot of the surface layer of the systems containing 5% HCN (left panel), 15% HCN (middle panel), and 30% HCN, shown from top view, the centers of the molecules being projected to the macroscopic plane of the surface, *YZ*. Water and HCN molecules are represented by red and green balls, respectively.

acetonitrile at the surface of its aqueous solutions was attributed to the dominance of dipolar interaction between the molecules at the vicinity of the interface.[36] Dipolar interactions can well be behind the multilayer adsorption behavior observed for HCN solutions, as well. This point is further addressed in a following subsection.

Comparing the mass density profiles of the entire systems with those of the first layers (Figure 2), it is seen that the first layer density peak extends well beyond the point where the density of the entire system already reaches the constant, bulk liquid phase value. This means that defining the interfacial region in the nonintrinsic way, i.e., as a slab of intermediate densities, would miss a large number of truly interfacial molecules (i.e., what can be seen from the vapor phase).

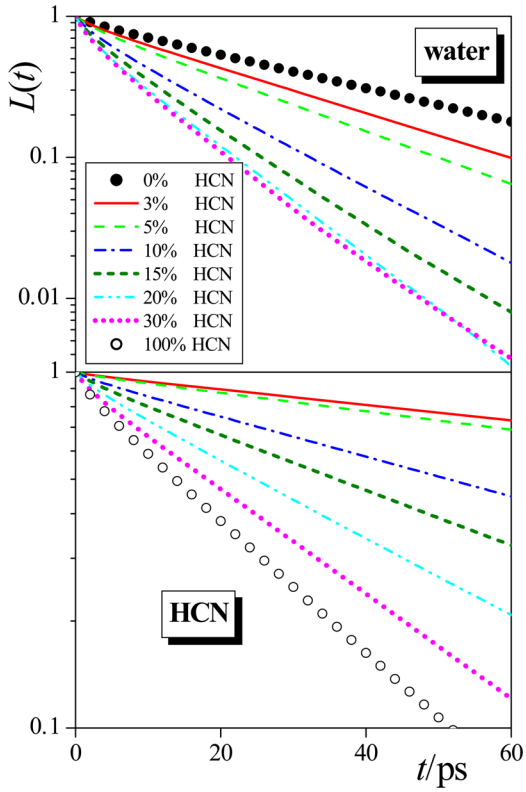

Figure 9. Survival probability of the water (top panel) and HCN (bottom panel) molecules in the surface layer of the systems containing 0% HCN (●), 3% HCN (red solid lines), 5% HCN (light green dashed lines), 10% HCN (dark blue dash−dotted lines), 15% HCN (dark green short dashed lines), 20% HCN (light blue dash−dot−dotted lines), 30% HCN (magenta dotted lines), and 100% HCN (○). To emphasize the exponential decay of the survival probabilities, the plot shows the data on a logarithmic scale.

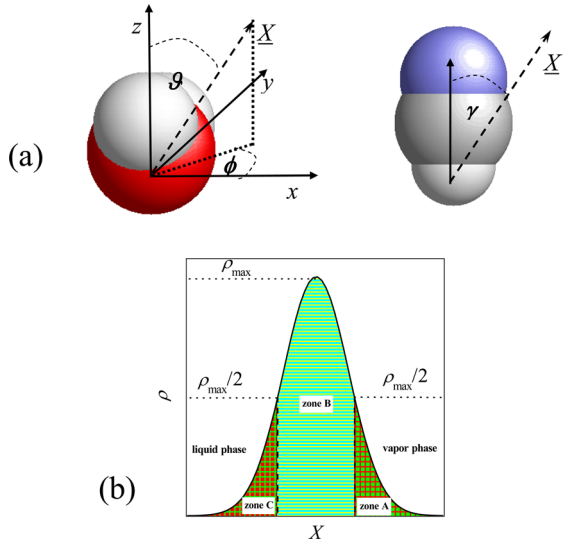

Figure 10. (a) Definition of the local Cartesian frame fixed to the individual surface water molecules (see the test) and the angles ϑ and ϕ (right), and γ (left), describing the surface orientation of the water and HCN molecules, respectively. O, H, C, and N atoms are shown by red, white, gray, and blue colors, respectively. (b) Illustration of the division of the surface layer into three separate zones, marked by A, B, and C (see the text).

dx.doi.org/10.1021/jp505978p | J. Phys. Chem. C 2014, 118, 21469−21482

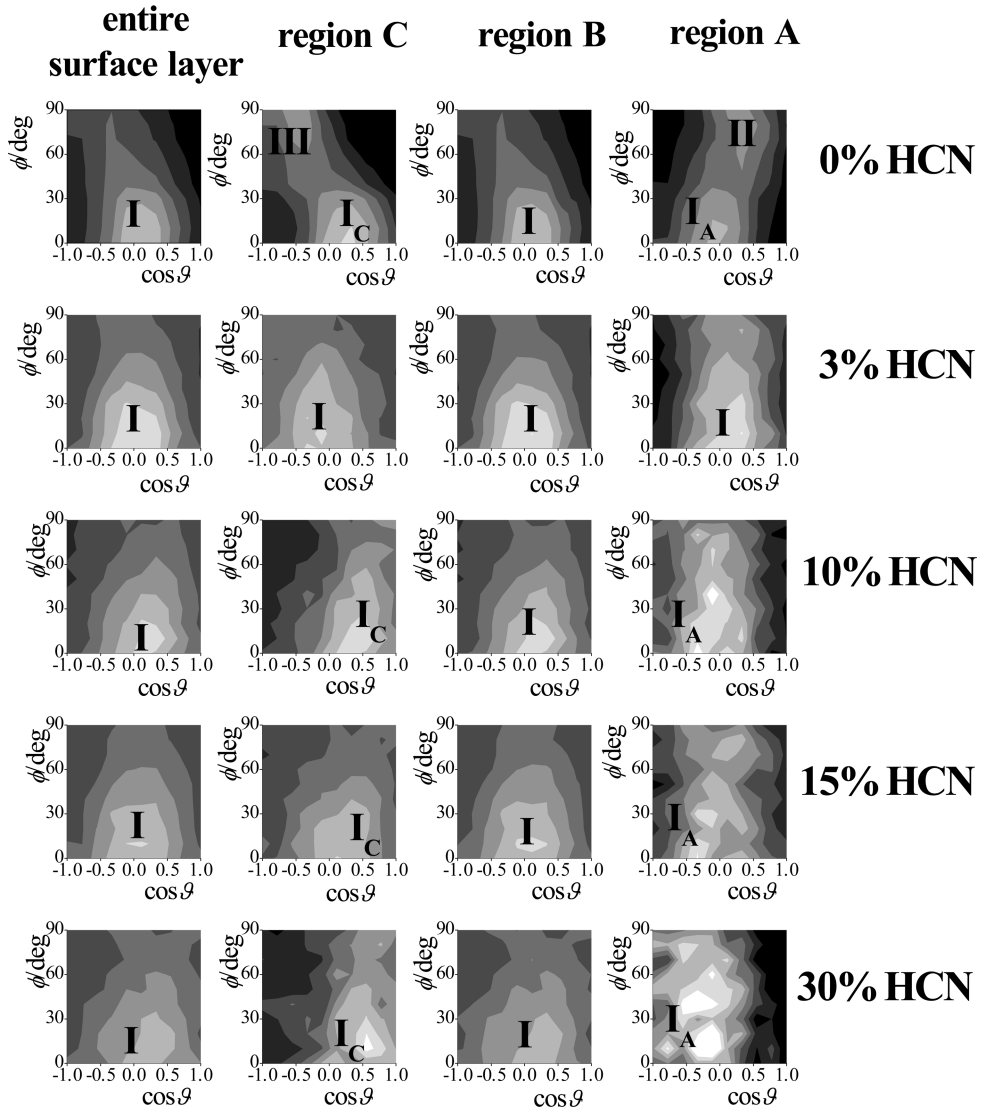

Figure 11. Orientational maps of the surface water molecules in the systems containing 0% HCN (top row), 3% HCN (second row), 10% HCN (third row), 15% HCN (fourth row), and 30% HCN (bottom row). The first column corresponds to the entire surface layer, whereas the second, third, and fourth columns to its separate zones C, B, and A, respectively. Lighter shades of gray indicate higher probabilities. The preferred water orientations corresponding to the different peaks of the $P(\cos\vartheta,\phi)$ orientational maps are also indicated.

Conversely, as seen from Figure 4, which shows the mass density profiles of the first three molecular layers along with that of the entire system in four selected mixed systems, the density peak of the second, and even that of the third layer, overlaps with the intermediate density part of the profile of the whole system. Thus, besides missing a large number of interfacial molecules, the nonintrinsic treatment of the interface would also misidentify a large number of molecules as being interfacial.

The density peaks corresponding to the individual subsurface molecular layers can be very well fitted by a Gaussian function in every case. Because the density profiles of the consecutive molecular layers are indeed supposed to follow Gaussian distributions,[70] this finding confirms the proper choice of the probe sphere radius in the ITIM analysis.[44] The width parameter of the fitted Gaussian function, δ, can serve as a measure of the width of the corresponding molecular layer, whereas the position of its center, X_c, is an estimate of the position of this layer. Thus, the difference of the X_c values of two consecutive layers, ΔX_c, characterizes the average separation of these layers. The δ and X_c values corresponding to the first three layers of the systems simulated are collected in Table 3. It is seen that, unlike in neat water, the first layer is always noticeably wider than the subsequent ones in HCN solutions, and this difference increases from about 2−3% to 6−8% with increasing HCN concentration. On the other hand, no tendentious difference is seen between the widths of the second and third subsurface molecular layers. Further, with increasing HCN concentration, all of the three subsurface layers become wider, as seen from the 20−30% increase of the corresponding δ parameters upon going from dilute to concentrated solutions. Similarly, the separation of the first two layers is always larger than that of the second and third layers, and this difference increases from about 3% to 10% upon going from dilute to concentrated solutions. Further, not only the difference between the separations of the first and second, and that of the second and third layers (i.e., $\Delta X_c(1-2) - \Delta X_c(1-3)$) increases with increasing HCN content, but also these interlayer separations (i.e., the ΔX_c values) themselves. All of these findings indicate that the molecules are less tightly packed

dx.doi.org/10.1021/jp505978p | J. Phys. Chem. C 2014, 118, 21469−21482

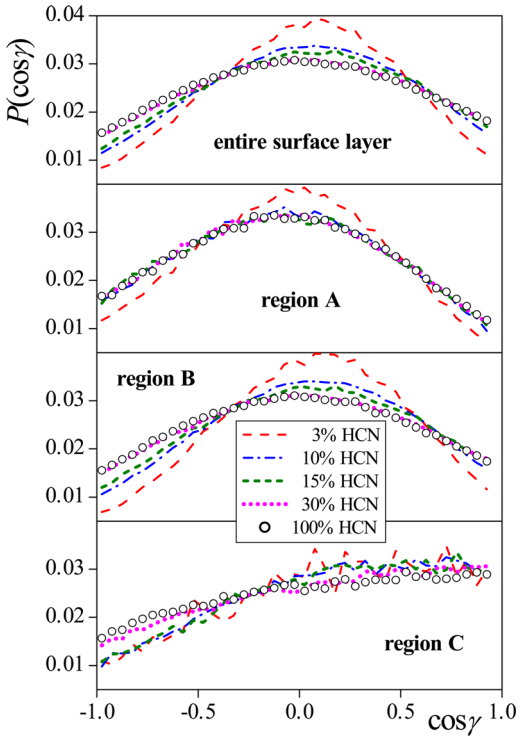

Figure 12. Cosine distribution of the angle γ, formed by the vector pointing from the H to the N atom of the surface HCN molecules and the macroscopic surface normal vector, X, pointing from the liquid to the vapor phase, in the systems containing 3% HCN (red solid lines), 10% HCN (blue dash−dotted lines), 15% HCN (green short dashed lines), 30% HCN (magenta dotted lines), and 100% HCN (○). The top panel corresponds to the entire surface layer, whereas the second, third, and fourth panels to its separate zones C, B, and A, respectively.

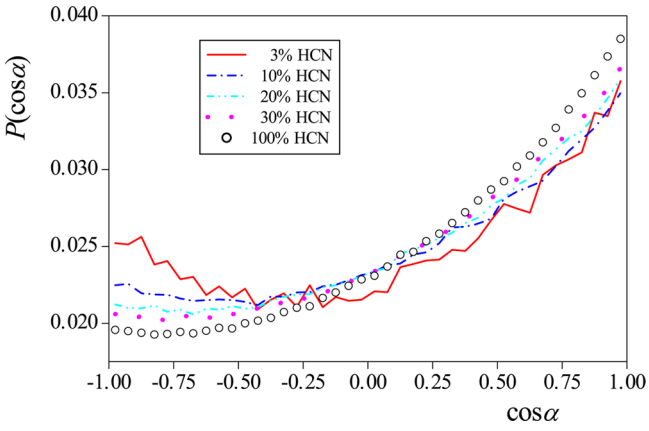

Figure 13. Cosine distribution of the angle α, formed by the vectors pointing from the H to the N atom of two neighboring surface HCN molecules, as obtained in the systems containing 3% HCN (red solid lines), 10% HCN (dark blue dash−dotted lines), 20% HCN (light blue dash−dot−dotted lines), 30% HCN (magenta dotted lines), and 100% HCN (○).

at the liquid surface than in the bulk liquid phase, and this effect is more pronounced around the HCN than around the water molecules. The reason for this less compact arrangement of the molecules at the interface is probably related to the fact that the orientational preferences of these molecules imposed by the vicinity of the vapor phase are not fully compatible with their tightly packed arrangement, which dominates in the bulk phase. The point concerning the interfacial orientation of the molecules is addressed in detail in a subsequent subsection.

Figure 5 compares the number density profiles of the water and HCN molecules in the surface layer of four selected mixed systems. The position of the molecules has been estimated by that of their O and C atoms, respectively. For better comparison, the two profiles are always scaled to each other. As is clear, the density peak of the HCN molecules is always shifted by 1.7−2.0 Å toward the vapor phase, as compared to the water density peak. This finding indicates that HCN is not only adsorbed at the first few molecular layers beneath the liquid surface, but even within the surface layer they are located noticeably closer to the vapor phase than the water molecules.

The ITIM algorithm not only identifies the full list of the surface molecules, but also provides a set of points that can serve as an estimate of the geometric covering surface of the liquid phase. This set of points can be determined from the positions at which the probe sphere is stopped along the different test lines.[33] Having the covering surface of the liquid phase already determined, its roughness can also be characterized. However, the description of the roughness of a known wavy surface is still not a trivial task, and it requires the use of at least two independent parameters, i.e., an amplitude-like and a frequency-like one.[33] For this purpose, we proposed to use the following parameter pair.[45] The average normal distance (i.e., distance along the macroscopic surface normal axis, X) of two surface points, $\bar{d}$, exhibits a saturation curve as a function of their lateral distance, l (i.e., distance in the macroscopic surface plane, YZ). The $\bar{d}(l)$ data can be well fitted by the function:

$$\bar{d}(l) = \frac{a\xi l}{a + \xi l} \tag{4}$$

The parameters ξ and a, corresponding to the steepness of the $\bar{d}(l)$ curve at small, and to its saturation value at large l values, respectively, can then serve as the frequency-like and amplitude-like roughness parameter, respectively. We have recently shown that the amplitude-like parameter, a, defined this way is closely related to the surface tension of the system.[71]

The $\bar{d}(l)$ roughness curves obtained in the systems simulated are shown in Figure 6, whereas the a and ξ parameters corresponding to all three subsurface layers are collected in Table 3. As is seen, with increasing HCN concentration the liquid surface gets rougher in terms of both frequency and amplitude, as the ξ and a parameters increase by about 15% and 30%, respectively, upon going from neat water to neat HCN. It is also seen that the surface layer is always somewhat rougher than the subsequent molecular layers, as the ξ parameter is about 15%, whereas a is about 8−10% larger in the first than in the second and third layers in every case. On the other hand, no considerable difference is seen between the roughness of the second and third layers in any case. This finding is illustrated by the inset of Figure 6, showing the $\bar{d}(l)$ data in the first three layers of the 3% HCN and 30% HCN systems, together with the curves fitted to them according to eq 4. The findings that (i) increasing HCN content leads to an increased roughness of the liquid surface, and (ii) the first layer is always rougher than the subsequent ones are perfectly in line with our previous observations concerning the width and separation of the subsequent molecular layers, and stress again that the molecules are less tightly packed at the liquid surface than in the bulk liquid phase, and this effect is more pronounced for the HCN than for the water molecules.

dx.doi.org/10.1021/jp505978p | J. Phys. Chem. C 2014, 118, 21469−21482

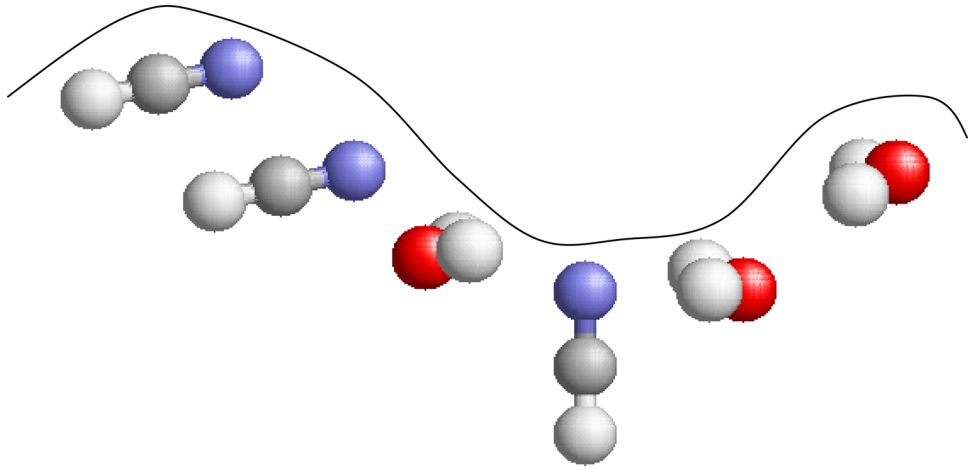

Figure 14. Illustration of the observed orientational preferences of the surface molecules relative to the macroscopic surface normal as well as to each other. The O, H, C, and N atoms of the water and HCN molecules are shown by red, white, gray, and blue colors, respectively.

3.2. Lateral Self-Association of the Surface Molecules. We have seen that HCN molecules are strongly adsorbed; i.e., their local concentration is considerably increased at the surface of their dilute aqueous solutions. Local HCN concentration can further increase within the surface layer by possible lateral self-association of the like molecules. Self-association in binary mixtures can be conveniently studied by Voronoi analysis.[72−74] In two-dimensional systems (e.g., liquid surfaces) of discrete seeds (e.g., molecules), the Voronoi polygon (VP) of a given seed is the locus of the points that are closer to this seed than to any other one. Further, the VP edges and vertices are loci of points having two and three closest seeds, respectively, at equal distances. Therefore, VP vertices are the centers of the largest circular vacancies (i.e., circles not containing any seed) in the system.[75,76] It has been shown that in the case of uniformly distributed seeds, the distribution of the VP area, A (or, in three dimensions that of the VP volume), is of Gaussian shape, whereas in cases when the seeds show large local density fluctuations the VP area distribution exhibits a long tail of exponential decay at large areas.[77] Taking this property into account, self-association in binary mixtures can be detected in the following way.[78] First, the VP area distribution of all of the seeds (molecules) is determined, to check that the molecules, irrespective of their type, are indeed uniformly distributed at the surface. Then, the VP area distribution is determined considering only one of the two components in the analysis, and completely disregarding the molecules of the other component. In case of self-association of the disregarded component, the area occupied by such self-aggregates is transformed into voids, and the VP area distribution of the component considered exhibits the exponential tail. This method has been successfully applied to detect self-association several times, both in two-[35−37] and three-dimensional[78,79] systems.

To investigate the possible self-association behavior of HCN molecules at the surface of their aqueous solutions, we have projected the centers (i.e., C or O atom) of all surface molecules to the macroscopic plane of the interface, YZ, and performed Voronoi analysis by considering both components as well as by disregarding one of them. The VP area distributions are shown in Figure 7 as obtained in selected systems. To emphasize the exponential character of the decay of the large area tails, the distributions are shown on a logarithmic scale. As is evident, there is a marked difference between the shape of the $P(A)$ distributions obtained by taking both components into account and by disregarding one of the components. In the first case, $P(A)$ is a narrow Gaussian, indicating, as expected, that surface molecules are uniformly distributed along the macroscopic plane of the surface. In the second case, however, the $P(A)$ distribution becomes very broad and exhibits an exponentially decaying tail (converted to a straight line by the logarithmic scale used) at large A values. It is also seen that the smaller is the concentration of a given component in the surface layer, the broader its $P(A)$ distribution becomes. All of these results indicate clearly that like components exhibit a strong tendency of self-association at the liquid surface of aqueous HCN solutions, and this self-association tendency is stronger for components of smaller concentration. The observed self-association behavior of the like molecules is illustrated in Figure 8, showing equilibrium snapshots of the surface layer of systems of three different compositions by projecting the center of the surface molecules to the macroscopic plane of the surface, YZ. Considering our above finding that surface HCN molecules tend to stay at the outer edge of the surface layer, the lateral self-associates of the surface HCN molecules can be regarded as patches floating at the surface of the liquid phase.

To quantify the extent of this self-association, one can determine the area of the largest circular voids when HCN molecules are disregarded from the analysis (as these voids are the surface portions that are covered by HCN self-aggregates), and compare this value to the average area occupied by a single HCN molecule (i.e., the mean value of $P(A)$ as obtained in the 100% HCN system). Having these values calculated, it turns out that HCN self-aggregates may consist of up to 8, 12, 25, 35, 55, and 150 molecules in the 3% HCN, 5% HCN, 10% HCN, 15% HCN, 20% HCN, and 30% HCN systems, i.e., when the bulk phase HCN concentration is about 0.8, 1.5, 2.8, 4.5, 5.5, and 8 M, respectively.

3.3. Dynamics of Exchange of the Molecules between the Surface and the Bulk. The dynamics of exchange of the molecules between the surface layer and bulk of the liquid phase can be characterized by the survival probability of the molecules in the surface layer, $L(t)$, i.e., the probability that a molecule that belongs to the surface layer at t_0 will stay at the surface up to $t_0 + t$. To distinguish between the situations when

dx.doi.org/10.1021/jp505978p | J. Phys. Chem. C 2014, 118, 21469−21482

the molecule leaves the surface permanently, and when it is only absent from the surface at a certain instant due to an oscillating move, departure of a molecule from the surface layer is allowed between t_0 and $t_0 + t$, given that it returns to the surface layer within Δt. Taking into account the typical time scale of such molecular oscillations, Δt is set here to its conventionally used value of 2 ps. Considering also that two consecutive sample configurations are always separated by a 1 ps long trajectory, this choice of Δt practically means that molecules are considered as though left the surface layer if they are absent from this layer in two consecutive sample configurations. To avoid any possible arbitrariness corresponding to the particular choice of Δt, we have repeated all the calculations with the Δt value of 1 ps (i.e., when the definition does not allow the molecules to be out of the surface layer even in a single sample configuration), but it did not change any of the conclusions of this analysis.

Because the permanent departure of the molecules from the surface layer is a process of first-order kinetics, the $L(t)$ data can be very well fitted by the exponentially decaying function $\exp(-t/\tau)$, where τ is the mean residence time of the molecules at the surface.

The $L(t)$ survival probabilities of the water and HCN molecules in the surface layer of the different systems simulated are shown in Figure 9, whereas the τ values corresponding to the first three subsurface molecular layers are included in Table 3. To emphasize the exponential decay of the survival probability, Figure 9 shows the obtained $L(t)$ data on a logarithmic scale. As is immediately seen, the τ values in the second and third layers are always an order of magnitude smaller than in the first layer, being comparable with the time window of Δt = 2 ps used in the analysis, indicating that defining the residence time in the second and subsequent molecular layers is physically already meaningless. In other words, the vicinity of the interface affects solely the first molecular layer beneath the liquid surface in this respect, whereas, from the dynamical point of view, the second subsurface molecular layer already belongs to the bulk liquid phase.

More importantly, it is seen that HCN molecules stay, on average, considerably longer at the liquid surface than the water molecules, and this difference is larger when the solution is more dilute. Thus, in the 3% HCN system, the mean residence time of the HCN molecules at the surface is about 8 times larger than that of the water molecules, whereas this ratio is only about 3 in the 30% HCN system. The mean residence time of the water molecules at the surface decreases parallel with that of the HCN molecules as the HCN concentration of the system increases. Thus, the presence of HCN speeds up the dynamics of exchange of the water molecules between the surface layer of the liquid phase and the bulk. These results indicate that in dilute solutions the HCN molecules are not only strongly adsorbed at the liquid surface, staying preferably at the outer edge of the surface layer, and exhibit strong lateral self-association resulting in large interfacial HCN clusters, but also stay for an unusually long time, an order of magnitude longer than water molecules, at the surface of the liquid phase. In other words, the floating patches of HCN are rather stable, staying at the liquid surface for a rather long time.

3.4. Surface Orientation. The orientation of a rigid molecule of general shape relative to an external direction (or plane) can only be described by two orientational variables, whereas that of molecules of $C_{\infty v}$ symmetry (e.g., linear ones) can already be described by one single variable. Therefore, the orientational statistics of the water molecules can be fully characterized only by the bivariate joint distribution of two independent orientational parameters,[80,81] while that of HCN can simply be described by the monovariate distribution of one single orientational parameter. For molecules of general shape, we have shown that the polar angles ϑ and ϕ of the macroscopic surface normal axis, $\underline{X}$, pointing, by our convention, toward the vapor phase, in a local Cartesian frame fixed to the individual molecules represent a sufficient choice of such a parameter pair.[80,81] Here, we define this local Cartesian frame of the water molecules in the following way. Its axis x is the molecular normal axis, axis y is parallel with the line joining the two H atoms, and axis z is the main symmetry axis of the molecule, directed to point from the O atom toward the H atoms along the molecular dipole vector. Because of the C_{2v} symmetry of the water molecule, this frame can always be chosen in such a way that the angle ϕ does not exceed 90°. Further, because ϑ is an angle of two general spatial vectors, but ϕ is formed by two vectors restricted to lay in a given plane (i.e., the xy plane of the molecular frame) by definition, uncorrelated orientation of the molecules with the surface plane results in constant distribution only if cos ϑ and ϕ are chosen to be the orientational variables. In the case of HCN, the situation is considerably simpler; here, we characterize the orientational statistics of the surface HCN molecules by the cosine distribution of the angle γ, formed by the vector pointing from the H to the N atom of the molecule and the macroscopic surface normal vector, $\underline{X}$, pointing from the liquid to the vapor phase. The definition of the local Cartesian frame fixed to the individual water molecules as well as that of the angles ϑ, ϕ, and γ are illustrated in Figure 10a.

It has been shown several times that the orientational preferences of the surface molecules strongly depend on the local curvature of the surface.[33−38,82] To take this effect also into account, we have divided the surface layer into three separate zones, marked by A, B, and C. Thus, zones A and C extend from the points where the mass density of the surface layer is one-half of its maximum value toward the vapor and the liquid phase, respectively, whereas zone B covers the X range where the mass density of the surface layer exceeds one-half of its maximum value. Thus, zones A and C typically cover the crests and troughs of the wavy liquid surface, i.e., surface portions of locally convex and concave curvature, respectively. The division of the surface layer into zones A, B, and C is illustrated in Figure 10b.

The $P(\cos\vartheta,\phi)$ orientational maps of the water molecules and the $P(\cos\gamma)$ orientational distributions of the HCN molecules are shown in Figures 11 and 12, respectively, as obtained in selected systems simulated. As it has been shown several times,[33,34] the molecules at the surface of neat water prefer to lay parallel with the plane of the macroscopic surface, as evidenced by the peak of the $P(\cos\vartheta,\phi)$ orientational map at cos ϑ = 0 and ϕ = 0°. This preferred orientation is marked here by I. In zones A and C, the peak corresponding to orientation I shifts to somewhat smaller (in zone A) and larger (in zone C) cos ϑ values, indicating that the water molecules prefer slightly tilted orientations, pointing by their H atoms flatly toward the bulk liquid phase in zone A and toward the vapor phase in zone C. These orientations are marked here as I_A and I_C. Further, in both of these zones, another orientation, characterized by the cos ϑ value of 0.5 (in zone A) and −0.5 (in zone C), and the ϕ value of 90° are preferred. In these orientations, denoted by II

dx.doi.org/10.1021/jp505978p | J. Phys. Chem. C 2014, 118, 21469−21482

and III, respectively, the water molecule stays perpendicular to the macroscopic plane of the surface, pointing by one of its O−H bonds straight toward the vapor phase (in zone A) and toward the bulk liquid phase (in zone C). These orientational preferences have been rationalized by considering that in zone A both preferred orientations are such that the water molecule "sacrifices" one of its four hydrogen-bonding directions (i.e., a lone pair direction in alignment I_A and an O−H direction in alignment II), and on this price it can form three stable hydrogen bonds in the other three, inward-oriented directions. On the other hand, in the orientations preferred in zone C, three hydrogen-bonding directions (i.e., one lone pair and two O−H directions in alignment I_C, and one O−H and two lone pair directions in alignment III) are straddling along the locally concave surface, maintaining thus all four hydrogen bonds of the water molecule.[33,34]

As is seen from Figure 11, in the presence of even a small amount of HCN, the preference for orientations II and III already vanishes, and the water molecules prefer nearly parallel alignment with the macroscopic surface plane everywhere within the surface layer. Correspondingly, the HCN molecules also prefer to lay almost parallel with the macroscopic plane of the surface, declining only by about 5−10° from it (see Figure 12). The only exception is zone C, where the N atom of the HCN molecule sticks preferentially out to the vapor phase. The preferred parallel alignment of both the water and the HCN molecules with the macroscopic surface plane allows strong dipolar interactions acting between neighbors within the surface layer, which can also explain the disappearance of the preference of the water molecules for the perpendicular alignments II and III.

To confirm the presence of considerable dipolar interactions within the surface layer, we have calculated the cosine distribution of the angle α, formed by the HN vector of two neighboring HCN molecules in the surface layer. (Two HCN molecules are regarded to be neighbors if their C atoms are closer than 6.0 Å, i.e., the first minimum position of the corresponding radial distribution function.[31]) The obtained $P(\cos\alpha)$ distributions, shown in Figure 13, exhibit their main peak at $\cos\alpha = 1$, indicating the clear preference of the neighboring HCN molecules for parallel relative alignment. Further, a small peak of $P(\cos\alpha)$ is seen at the $\cos\alpha$ value of −1, being larger in more dilute systems, indicating the secondary preference of the neighboring HCN molecules for antiparallel relative alignment. All of these orientational preferences are illustrated in Figure 14.

The observed preferred relative alignment of the neighboring surface HCN molecules is in a full accord with the assumed strong dipolar interactions within the surface layer. These dipolar interactions can further stabilize the HCN patches floating at the liquid surface, and can be, at least partly, responsible for the unusually long residence time of the HCN molecules in the surface layer.

4. SUMMARY AND CONCLUSIONS

In this Article, we presented a detailed investigation of the intrinsic surface of aqueous HCN solutions of different concentrations by means of molecular dynamics computer simulation and ITIM analysis. One of the most important findings of this study is that HCN molecules are strongly adsorbed at the surface of the liquid phase despite the full miscibility of HCN with water. Thus, in dilute solutions, even about an order of magnitude larger HCN concentrations can be found at the surface layer than in the bulk liquid phase. In addition, the larger is the bulk phase HCN concentration, the more subsurface layers are involved in HCN adsorption, resulting in significant enrichment of HCN also in the second and third subsurface molecular layers as compared to the bulk liquid phase. Another interesting feature of the surface HCN molecules is that they prefer to stay at the outer edge of the surface layer, being noticeably closer to the vapor phase than the surface water molecules. Also, all three subsurface layers become wider with increasing HCN concentration. As a consequence of this chaotropic nature of HCN, the molecules are less tightly packed at the liquid surface than in the bulk liquid phase, and hence the liquid surface gets rougher with increasing HCN concentration.

Besides the aforementioned strong adsorption, the local HCN concentration is found to be even further increased at certain patches of the liquid surface by the strong self-association tendency of the like molecules, detected by Voronoi analysis of the surface layer. Furthermore, the mean residence time of the HCN molecules at the liquid surface is found to be considerably longer than that of the water molecules, and the more dilute is the solution, the longer HCN molecules can stay at the liquid surface. All of these findings indicate that the HCN molecules can form long-lasting HCN patches floating at the surface of their aqueous solutions, even at low bulk phase concentrations.

This finding has important consequences regarding the "HCN world" hypothesis,[15,26] the main argument against which is that polymerization of HCN and thus the formation of adenine can only occur in concentrated (1−11 M) solutions.[27,28] The present results show, however, that HCN concentration can be very high at certain patches of even its dilute aqueous solutions, and such floating HCN patches can be considered to have formed by spontaneous process in the primordial time. These floating HCN patches might provide spots for polymerization of HCN, which could finally lead to the dawn of the prebiotic biomolecular building blocks, such as adenine. Therefore, adenine might well form at the surface of dilute HCN solutions due to the locally strongly enhanced HCN concentration, and it is also sensible to assume that most of the adenine molecules being formed this way stay there, because adenine is only partially miscible with water.

■ ASSOCIATED CONTENT

Supporting Information

Complete refs 1, 2, 5−7, 9. This material is available free of charge via the Internet at http://pubs.acs.org.

■ AUTHOR INFORMATION

Corresponding Authors

*E-mail: milan@jgypk.u-szeged.hu.
*E-mail: pali@chem.elte.hu.

Notes

The authors declare no competing financial interest.

■ ACKNOWLEDGMENTS

This project is supported by the Hungarian OTKA Foundation under project no. 104234. P.J. is a Szentágothai János fellow of NKPR, which is gratefully acknowledged. M.Sz. is a Magyary Zoltán fellow, and P.J. is a Szentágothai János fellow of Hungary, supported by State of Hungary and the European Union, cofinanced by the European Social Fund in the

framework of TÁMOP 4.2.4.A/2-11-1-2012-0001 "National Excellence Program" under the respective grant numbers of A2-MZPD-12-0139 (M.Sz.) and A2-SZJÖ-TOK-13-0030 (P.J.). Infrastructural support was provided by the TÁMOP-4.2.2.A-11/1/KONV-2012-0047, "New Functional Materials and Their Biological and Environmental Answers", and TÁMOP-4.2.2/C-11/1/KONV-2012-0010 cofinanced by the European Union and the European Social Fund.

REFERENCES

(1) Rinsland, C. P.; Goldman, A.; Mucray, F. J.; Stephen, T. M.; Pougatchev, N. S.; Fishman, J.; David, S. J.; Blatherwick, R. D.; Novelli, P. C.; Jones, N. B.; et al. Infrared Solar Spectroscopic Measurements of Free Tropospheric CO, C_2H_6, and HCN above Mauna Loa, Hawaii: Seasonal Variations and Evidence for Enhanced Emissions from the Southeast Asian Tropical Fires of 1997−1998. *J. Geophys. Res.: Atmos.* **1999**, *104*, 18667−18680.

(2) Singh, H. B.; Salas, L.; Herlth, D.; Kolyer, R.; Czech, E.; Viezee, W.; Li, Q.; Jacob, D. J.; Blake, D.; Sachse, G.; et al. In Situ Measurements of HCN and CH_3CN over the Pacific Ocean: Sources, Sinks, and Budgets. *J. Geophys. Res.: Atmos.* **2003**, *108*, GTE16-1−14.

(3) Li, Q.; Jacob, D. J.; Yantosca, R. M.; Heald, C. L.; Singh, H. B.; Koike, M.; Zhao, Y.; Sachse, G. W.; Streets, D. G. A Global Three-Dimensional Model Analysis of the Atmospheric Budgets of HCN and CH3CN: Constraints from Aircraft and Ground Measurements. *J. Geophys. Res.: Atmos* **2003**, *108*, GTE48-1−13.

(4) Akagi, S. K.; Yokelson, R. J.; Wiedinmyer, C.; Alvarado, M. J.; Reid, J. S.; Karl, T.; Crounse, J. D.; Wennberg, P. O. Emission Factors for Open and Domestic Biomass Burning for Use in Atmospheric Models. *Atmos. Chem. Phys.* **2011**, *11*, 4039−4072.

(5) Singh, H. B.; Salas, L.; Herlth, D.; Kolyer, R.; Czech, E.; Avery, M.; Crawford, J. H.; Pierce, R. B.; Sachse, G. W.; Blake, D. R.; et al. Reactive Nitrogen Distribution and Partitioning in the North American Troposphere and Lowermost Stratosphere. *J. Geophys. Res.: Atmos.* **2007**, *112*, D12S04-1−15.

(6) Liang, Q.; Jaeglé, L.; Hudman, R. C.; Turquety, S.; Jacob, D. J.; Avery, M. A.; Browell, E. V.; Sachse, G. W.; Blake, D. R.; Brune, W.; et al. Summertime Influence of Asian Pollution in the Free Troposphere over North America. *J. Geophys. Res.: Atmos.* **2007**, *112*, D12S11-1−20.

(7) Le Breton, M.; Bacak, A.; Muller, J. B. A.; O'Shea, S. J.; Xiao, P.; Ashfold, M. N. R.; Cooke, M. C.; Batt, R.; Shallcross, D. E.; Oram, D. E.; et al. Airborne Hydrogen Cyanide Measurements Using a Chemical Ionisation Mass Spectrometer for the Plume Identification of Biomass Burning Forest Fires. *Atmos. Chem. Phys.* **2013**, *13*, 9217−9232.

(8) Kleinböhl, A.; Toon, G. C.; Shen, B.; Blavier, J. F. L.; Weisenstein, D. K.; Strekowski, R. S.; Nicovich, J. M.; Wine, P. H.; Wennberg, P. O. On the Stratospheric Chemistry of Hydrogen Cyanide. *Geophys. Res. Lett.* **2006**, *33*, L11806-1−5.

(9) Bernath, P. F.; McElroy, C. T.; Abrams, M. C.; Boone, C. D.; Butler, M.; Camy-Peyret, C.; Carleer, M.; Clerbaux, C.; Coheur, P. F.; Colin, R.; et al. Atmospheric Chemistry Experiment (ACE): Mission O verview. *Geophys. Res. Lett.* **2005**, *32*, L15S01-1−5.

(10) Randel, W. J.; Park, M.; Emmons, L.; Kinnison, D.; Bernath, P.; Walker, K. A.; Boone, C.; Pumphrey, H. Asian Monsoon Transport of Pollution to the Stratosphere. *Science* **2010**, *328*, 611−613.

(11) Li, Q.; Jacob, D. J.; Bey, I.; Yantosca, R. M.; Zhao, Y.; Kondo, Y.; Notholt, J. Atmospheric Hydrogen Cyanide (HCN): Biomass Burning Source, Ocean Sink? *Geophys. Res. Lett.* **2000**, *27*, 357−360.

(12) Bunkan, A. J. C.; Liang, C. H.; Pilling, M. J.; Nielsen, C. J. Theoretical and Experimental Study of the OH Radical Reaction with HCN. *Mol. Phys.* **2013**, *111*, 1589−1598.

(13) Miller, S. L. A Production of Amino Acids under Possible Primitive Earth Conditions. *Science* **1953**, *117*, 528−529.

(14) Matthews, C. N.; Moser, R. E. Peptide Synthesis from Hydrogen Cyanide and Water. *Nature* **1967**, *215*, 1230−1234.

(15) Matthews, C. N. In *Origins: Genesis, Evolution and Diversity of Life* (Series: Cellular Origin and Life in Extreme Habitats and Astrobiology, Vol. *6*); Seckbach, J., Ed.; Kluwer: Dordrecht, 2004; pp 121−135.

(16) Ferris, J. P.; Hagan, W. J. HCN and Chemical Evolution: The Possible Role of Cyano Compounds in Prebiotic Synthesis. *Tetrahedron* **1984**, *40*, 1093−1120.

(17) Barnun, A.; Shaviv, A. Dynamics of Chemical Evolution of Earths Primitive Atmosphere. *Icarus* **1975**, *24*, 197−210.

(18) Ferris, J. P.; Joshi, P. C.; Edelson, E. H.; Lawless, J. G. HCN: A Plausible Source of Purines, Pyrimidines and Amino Acids on the Primitive Earth. *J. Mol. Evol.* **1978**, *11*, 293−311.

(19) Schwartz, A. W. Intractable mixtures and the origin of life. *Chem. Biodiversity* **2007**, *4*, 656−664.

(20) Eschenmoser, A. On a hypothetical generational relationship between HCN and constituents of the reductive citric acid cycle. *Chem. Biodiversity* **2007**, *4*, 554−573.

(21) Holm, N. G.; Neubeck, A. Reduction of Nitrogen Compounds in Oceanic Basement and its Implications for HCN Formation and Abiotic Organic Synthesis. *Geochem. Trans.* **2009**, *10*, 9-1−11.

(22) Szőri, M.; Jójárt, B.; Izsák, R.; Szőri, K.; Csizmadia, I. G.; Viskolcz, B. Chemical Evolution of Biomolecule Building Blocks. Can Thermodynamics Explain the Accumulation of Glycine in the Prebiotic Ocean? *Phys. Chem. Chem. Phys.* **2011**, *13*, 7449−7458.

(23) Miyakawa, S.; Cleaves, H. J.; Miller, S. L. The Cold Origin of Life: A. Implications Based on the Hydrolytic Stabilities of Hydrogen Cyanide and Formamide. *Origins Life Evol. Biospheres* **2002**, *32*, 195−208.

(24) Holm, N. G.; Neubeck, A. Reduction of Nitrogen Compounds in Oceanic Basement and its Implications for HCN Formation and Abiotic Organic Synthesis. *Geochem. Trans.* **2009**, *10*, 9-1−11.

(25) Roy, D.; Najafian, K.; von Ragué Schleyer, P. Chemical Evolution: The Mechanism of the Formation of Adenine under Prebiotic Conditions. *Proc. Natl. Acad. Sci. U.S.A.* **2007**, *104*, 17272−17277.

(26) Minard, R. D.; Matthews, C. N. HCN World: Establishing Proteininucleic Acid Life via Hydrogen Cyanide Polymers. *Abstr. Pap., Am. Chem. Soc.* **2004**, *228*, U963−U963.

(27) Oró, J.; Kamat, J. S. Amino-acid Synthesis from Hydrogen Cyanide under Possible Primitive Earth Conditions. *Nature* **1961**, *190*, 442−443.

(28) Oró, J.; Kimball, A. P. Synthesis of Purines under Possible Primitive Earth Conditions: II. Purine Intermediates from Hydrogen Cyanide. *Arch. Biochem. Biophys.* **1962**, *96*, 293−313.

(29) Saladino, R.; Crestini, C.; Pinto, S.; Costanzo, G.; Di Mauro, E. Formamide and the Origin of Life. *Phys. Life Rev.* **2012**, *9*, 84−104.

(30) Stribling, R.; Miller, S. L. Energy Yields for Hydrogen-Cyanide and Formaldehyde Syntheses - the HCN and Amino-Acid-Concentrations in the Primitive Ocean. *Origins Life Evol. Biospheres* **1987**, *17*, 261−273.

(31) Szőri, M.; Jedlovszky, P. Adsorption of HCN at the Surface of Ice: A Grand Canonical Monte Carlo Simulation Study. *J. Phys. Chem. C* **2014**, *118*, 3599−3609.

(32) Wick, C. D. HCl Accommodation, Dissociation, and Propensity for the Surface of Water. *J. Phys. Chem. A* **2013**, *117*, 12459−12467.

(33) Pártay, L. B.; Hantal, Gy.; Jedlovszky, P.; Vincze, Á.; Horvai, G. A New Method for Determining the Interfacial Molecules and Characterizing the Surface Roughness in Computer Simulations. Application to the Liquid−Vapor Interface of Water. *J. Comput. Chem.* **2008**, *29*, 945−956.

(34) Hantal, Gy.; Darvas, M.; Pártay, L. B.; Horvai, G.; Jedlovszky, P. Molecular Level Properties of the Free Water Surface and Different Organic Liquid/Water Interfaces, as Seen from ITIM Analysis of Computer Simulation Results. *J. Phys.: Condens. Matter* **2010**, *22*, 284112-1−14.

(35) Pártay, L. B.; Jedlovszky, P.; Vincze, Á.; Horvai, G. Properties of Free Surface of Water-Methanol Mixtures. Analysis of the Truly Interfacial Molecular Layer in Computer Simulation. *J. Phys. Chem. B* **2008**, *112*, 5428−5438.

(36) Pártay, L. B.; Jedlovszky, P.; Horvai, G. Structure of the Liquid-Vapor Interface of Water-Acetonitrile Mixtures As Seen from

Molecular Dynamics Simulations and Identification of Truly Interfacial Molecules Analysis. *J. Phys. Chem. C* **2009**, *113*, 18173−18183.
(37) Pojják, K.; Darvas, M.; Horvai, G.; Jedlovszky, P. Properties of the Liquid-Vapor Interface of Water-Dimethyl Sulfoxide Mixtures. A Molecular Dynamics Simulation and ITIM Analysis Study. *J. Phys. Chem. C* **2010**, *114*, 12207−12220.
(38) Pártay, L. B.; Horvai, G.; Jedlovszky, P. Temperature and Pressure Dependence of the Properties of the Liquid-Liquid Interface. A Computer Simulation and Identification of the Truly Interfacial Molecules Investigation of the Water-Benzene System. *J. Phys. Chem. C* **2010**, *114*, 21681−21693.
(39) Chacón, E.; Tarazona, P. Intrinsic Profiles beyond the Capillary Wave Theory: A Monte Carlo Study. *Phys. Rev. Lett.* **2003**, *91*, 166103-1−4.
(40) Chacón, E.; Tarazona, P. Characterization of the Intrinsic Density Profiles for Liquid Surfaces. *J. Phys.: Condens. Matter* **2005**, *17*, S3493−S3498.
(41) Chowdhary, J.; Ladanyi, B. M. Water-Hydrocarbon Interfaces: Effect of Hydrocarbon Branching on Interfacial Structure. *J. Phys. Chem. B* **2006**, *110*, 15442−15453.
(42) Jorge, M.; Cordeiro, M. N. D. S. Intrinsic Structure and Dynamics of the Water/Nitrobenzene Interface. *J. Phys. Chem. C* **2007**, *111*, 17612−17626.
(43) Sega, M.; Kantorovich, S.; Jedlovszky, P.; Jorge, M. The Generalized Identification of Truly Interfacial Molecules (ITIM) Algorithm for Nonplanar Interfaces. *J. Chem. Phys.* **2013**, *138*, 044110-1−10.
(44) Jorge, M.; Jedlovszky, P.; Cordeiro, M. N. D. S. A Critical Assessment of Methods for the Intrinsic Analysis of Liquid Interfaces. 1. Surface Site Distributions. *J. Phys. Chem. C* **2010**, *114*, 11169−11179.
(45) Darvas, M.; Pártay, L. B.; Jedlovszky, P.; Horvai, G. Computer Simulation and ITIM Analysis of the Surface of Water-Methanol Mixtures Containing Traces of Water. *J. Mol. Liq.* **2012**, *153*, 88−93.
(46) Darvas, M.; Pojják, K.; Horvai, G.; Jedlovszky, P. Molecular Dynamics Simulation and Identification of the Truly Interfacial Molecules (ITIM) Analysis of the Liquid-Vapor Interface of Dimethyl Sulfoxide. *J. Chem. Phys.* **2010**, *132*, 134701-1−10.
(47) Hantal, G.; Cordeiro, M. N. D. S.; Jorge, M. What Does an Ionic Liquid Surface Really Look Like? Unprecedented Details from Molecular Simulations. *Phys. Chem. Chem. Phys.* **2011**, *13*, 21230−21232.
(48) Lísal, M.; Posel, Z.; Izák, P. Air−Liquid Interfaces of Imidazolium-Based $[TF_2N^-]$ Ionic Liquids: Insight from Molecular Dynamics Simulations. *Phys. Chem. Chem. Phys.* **2012**, *14*, 5164−5177.
(49) Hantal, G.; Voroshylova, I.; Cordeiro, M. N. D. S.; Jorge, M. A Systematic Molecular Simulation Study of Ionic Liquid Surfaces Using Intrinsic Analysis Methods. *Phys. Chem. Chem. Phys.* **2012**, *14*, 5200−5213.
(50) Lísal, M. The Liquid Surface of Chiral Ionic Liquids as Seen from Molecular Dynamics Simulations Combined with Intrinsic Analysis. *J. Chem. Phys.* **2013**, *139*, 214701-1−15.
(51) Pártay, L. B.; Horvai, G.; Jedlovszky, P. Molecular Level Structure of the Liquid/Liquid Interface. Molecular Dynamics Simulation and ITIM Analysis of the Water-CCl_4 System. *Phys. Chem. Chem. Phys.* **2008**, *10*, 4754−4764.
(52) Hantal, G.; Terleczky, P.; Horvai, G.; Nyulászi, L.; Jedlovszky, P. Molecular Level Properties of the Water-Dichloromethane Liquid/Liquid Interface, as Seen from Molecular Dynamics Simulation and Identification of Truly Interfacial Molecules Analysis. *J. Phys. Chem. C* **2009**, *113*, 19263−10276.
(53) Darvas, M.; Jorge, M.; Cordeiro, M. N. D. S.; Kantorovich, S. S.; Sega, M.; Jedlovszky, P. Calculation of the Intrinsic Solvation Free Energy Profile of an Ionic Penetrant Across a Liquid/Liquid Interface with Computer Simulations. *J. Phys. Chem. B* **2013**, *117*, 16148−16156.
(54) Darvas, M.; Jorge, M.; Cordeiro, M. N. D. S.; Jedlovszky, P. Calculation of the Intrinsic Solvation Free Energy Profile of Methane across a Liquid/Liquid Interface in Computer Simulations. *J. Mol. Liq.* **2014**, *189*, 39−43.
(55) Sega, M.; Horvai, G.; Jedlovszky, P. Microscopic Origin of the Surface Tension Anomaly of Water. *Langmuir* **2014**, *30*, 2969−2972.
(56) Kotdawala, R. R.; Ozgur Yazaydin, A.; Kazantzis, N.; Thompson, R. W. A Molecular Simulation Approach to the Study of Adsorption of Hydrogen Cyanide and Methyl Ethyl Ketone in Silicalite, Mordenite and Zeolite Beta Structures. *Mol. Simul.* **2007**, *33*, 843−850.
(57) Jorgensen, W. L.; Briggs, J. M. Monte Carlo Simulations of Liquid Acetonitrile with a Three-Site Model. *Mol. Phys.* **1988**, *63*, 547−558.
(58) Jorgensen, W. L.; Maxwell, D. S.; Tirado-Rives, J. Development and Testing of the OPLS All-Atom Force Field on Conformational Energetics and Properties of Organic Liquids. *J. Am. Chem. Soc.* **1996**, *118*, 11225−11236.
(59) Martiniano, H. F. M. C.; Cabral, B. J. C. Structure and Electronic Properties of a Strong Dipolar Liquid: Born-Oppenheimer Molecular Dynamics of Liquid Hydrogen Cyanide. *Chem. Phys. Lett.* **2013**, *555*, 119−124.
(60) Jorgensen, W. L.; Chandrashekar, J.; Madura, J. D.; Impey, R.; Klein, M. L. Comparison of Simple Potential Functions for Simulating Liquid Water. *J. Chem. Phys.* **1983**, *79*, 926−935.
(61) Allen, M. P.; Tildesley, D. J. *Computer Simulation of Liquids*; Clarendon Press: Oxford, 1987.
(62) Essman, U.; Perera, L.; Berkowitz, M. L.; Darden, T.; Lee, H.; Pedersen, L. G. A Smooth Particle Mesh Ewald Method. *J. Chem. Phys.* **1995**, *103*, 8577−8594.
(63) Hess, B.; Kutzner, C.; van der Spoel, D.; Lindahl, E. GROMACS 4: Algorithms for Highly Efficient, Load-Balanced, and Scalable Molecular Simulation. *J. Chem. Theory Comput.* **2008**, *4*, 435−447.
(64) Nosé, S. A Molecular Dynamics Method for Simulations in the Canonical Ensemble. *Mol. Phys.* **1984**, *52*, 255−268.
(65) Hoover, W. G. Canonical Dynamics: Equilibrium Phase-Space Distributions. *Phys. Rev. A* **1985**, *31*, 1695−1697.
(66) Hess, B. P-LINCS: A Parallel Linear Constraint Solver for Molecular Simulation. *J. Chem. Theory Comput.* **2008**, *4*, 116−122.
(67) Miyamoto, S.; Kollman, P. A. Settle: An Analytical Version of the SHAKE and RATTLE Algorithm for Rigid Water Models. *J. Comput. Chem.* **1992**, *13*, 952−962.
(68) Fujii, H.; Matsumoto, T.; Ueda, T.; Nogi, K. A New Method for Simultaneous Measurement of Surface Tension and Viscosity. *J. Mater. Sci.* **2005**, *40*, 2161−2166.
(69) Salem, H.; Katz, S. A. *Inhalation Toxicology*; CRC Press: Boca Raton, FL, 2005; p 719.
(70) Chowdhary, J.; Ladanyi, B. M. Surface Fluctuations at the Liquid-Liquid Interface. *Phys. Rev. E* **2008**, *77*, 031609.
(71) Jedlovszky, P.; Darvas, M.; Horvai, G. Relation between the Surface Tension and Roughness of the Intrinsic Liquid Surface. *Z. Naturforsch., A* **2013**, *68*, 123−129.
(72) Voronoi, G. F. Recherches sur le Paralléloèders Primitives. *J. Reine Angew. Math.* **1908**, *134*, 198−287.
(73) Medvedev, N. N. *The Voronoi-Delaunay Method in the Structural Investigation of Non-Crystalline Systems*; SB RAS: Novosibirsk, 2000; in Russian.
(74) Okabe, A.; Boots, B.; Sugihara, K.; Chiu, S. N. *Spatial Tessellations: Concepts and Applications of Voronoi Diagrams*; John Wiley: Chichester, 2000.
(75) Baranyai, A.; Ruff, I. Statistical Geometry of Molten Alkali Halides. *J. Chem. Phys.* **1986**, *85*, 365−373.
(76) Ruff, I.; Baranyai, A.; Pálinkás, G.; Heinzinger, K. Grand Canonical Monte Carlo Simulation of Liquid Argon. *J. Chem. Phys.* **1986**, *85*, 2169−2177.
(77) Zaninetti, L. The Voronoi Tessalation Generated from Different Distributions of Seeds. *Phys. Lett. A* **1992**, *165*, 143−147.
(78) Idrissi, A.; Damay, P.; Yukichi, K.; Jedlovszky, P. Self-Association of Urea in Aqueous Solutions: A Voronoi Polyhedron Analysis Study. *J. Chem. Phys.* **2008**, *129*, 164512−1−9.
(79) Idrissi, A.; Polok, K.; Gadomski, W.; Vyalov, I.; Agapov, A.; Kiselev, M.; Barj, M.; Jedlovszky, P. Detailed Insight into the

Hydrogen Bonding Interactions in Acetone−Methanol Mixtures. A Molecular Dynamics Simulation and Voronoi Polyhedra Analysis Study. *Phys. Chem. Chem. Phys.* **2012**, *14*, 5979−5987.
(80) Jedlovszky, P.; Vincze, Á.; Horvai, G. New Insight into the Orientational Order of Water Molecules at the Water/1,2-Dichloroethane Interface: A Monte Carlo Simulation Study. *J. Chem. Phys.* **2002**, *117*, 2271−2280.
(81) Jedlovszky, P.; Vincze, Á.; Horvai, G. Full Description of the Orientational Statistics of Molecules Near to Interfaces. Water at the Interface with CCl_4. *Phys. Chem. Chem. Phys.* **2004**, *6*, 1874−1879.
(82) Jedlovszky, P.; Předota, M.; Nezbeda, I. Hydration of Apolar Solutes of Varying Size: A Systematic Study. *Mol. Phys.* **2006**, *104*, 2465−2476.